White Rose Research Online

eprints@whiterose.ac.uk
https://eprints.whiterose.ac.uk
Universities of Leeds, Sheffield and York

Deposited via The University of Sheffield.

White Rose Research Online URL for this paper:
https://eprints.whiterose.ac.uk/id/eprint/246128/

Version: Published Version

Article:
Coldman, S., Zhou, G., Wu, D. et al. (2026) Segmentation repeatability and correlation of texture and shape features with gestational age in MRI of healthy placenta, placenta previa, and placenta accreta spectrum. British Journal of Radiology. tqag194. ISSN: 0007-1285

https://doi.org/10.1093/bjr/tqag194

Reuse
This article is distributed under the terms of the Creative Commons Attribution (CC BY) licence. This licence allows you to distribute, remix, tweak, and build upon the work, even commercially, as long as you credit the authors for the original work. More information and the full terms of the licence here: https://creativecommons.org/licenses/

Takedown
If you consider content in White Rose Research Online to be in breach of UK law, please notify us by emailing eprints@whiterose.ac.uk including the URL of the record and the reason for the withdrawal request.

UNIVERSITY OF LEEDS
University of Sheffield
UNIVERSITY of York

BJR, 2026, 00, 1–12
https://doi.org/10.1093/bjr/tqag194
Advance access publication: 21 August 2026
Research Article

BIR British Institute of Radiology
OXFORD

Segmentation repeatability and correlation of texture and shape features with gestational age in MRI of healthy placenta, placenta previa, and placenta accreta spectrum

Suzie Coldman, MSc[1,2,*], Guanglong Zhou, MSc[1,2], Dengjiang Wu, MSc[1,2], Lingzhong Guo, PhD[1,2], Elspeth Whitby, PhD[3], Xinshan Li, PhD[1,2]

[1]University of Sheffield, Sheffield City Centre, Sheffield, S1 3JD, United Kingdom
[2]Insigneo Institute for Healthcare Technology, Sheffield, S1 3JD, United Kingdom
[3]Sheffield Teaching Hospitals NHS Foundation Trust, Royal Hallamshire Hospital, Sheffield S10 2JF, United Kingdom
*Corresponding author: Suzie Coldman, MSc, Insigneo Institute for Healthcare Technology, University of Sheffield, C + 14, Pam Liversidge Building, Sir Frederick Mappin Building, Mappin Street, Sheffield City Centre, Sheffield S1 3JD, United Kingdom (slcoldman1@sheffield.ac.uk).

Abstract

Objectives: **To determine the most repeatable anatomical plane for placental segmentation and investigate any correlation between gestational age (GA) and texture and shape features of healthy placenta, placenta previa (PP) and placenta accreta spectrum (PAS).**

Methods: **T2 MRIs from 190 women with PP, PAS and healthy placenta were collected from a single center. Intra- and inter-observer studies were conducted by 3 operators, each manually segmenting 3 times in the sagittal, coronal, and axial planes. Two thousand five hundred and twenty-five texture and shape features were extracted from each MRI using PyRadiomics, and their correlation with GA determined using Spearman's correlation coefficient (ρ).**

Results: **For the segmentation study, 3 healthy and 3 PAS pregnancies were investigated. The sagittal plane exhibited the highest median dice coefficient (DC) in the intra-observer study for PAS (0.915) and inter-observer study for healthy (0.907) and PAS (0.891). For correlation with GA, 46 healthy, 49 PAS, and 57 PP MRIs were utilized. Texture features like grey level non-uniformity exhibited strong correlations with GA in the healthy group (ρ = 0.81, $P < .001$), but only moderate correlations in the PP (ρ = 0.58, $P < .001$) and PAS (ρ = 0.52, $P < .001$) groups.**

Conclusion: **The sagittal plane was the most repeatable anatomical plane for manually segmenting healthy placenta and PAS. Texture features describing heterogeneity were correlated with GA, particularly in healthy placenta.**

Advances in knowledge: **Texture and shape features captured the increase in heterogeneity seen throughout gestation on placental MRI, indicating a need to consider GA when investigating textural differences in healthy placentas, PP, and PAS.**

Key words placenta, placenta accreta spectrum, MRI, segmentation, gestational age, texture analysis

Introduction

Placenta accreta spectrum (PAS) is the incorrect attachment of the placenta to the uterine wall, often leading to a post-partum hemorrhage (PPH).[1-3] Its incidence has increased 10-fold in the last 4 decades, owing to the increasing rates of cesarean delivery and maternal age.[3-6] In many NHS hospitals, diagnosis involves MRI indications such as dark intraplacental bands.[7] In literature, this has demonstrated good sensitivity (0.83-0.89) and specificity (0.83-0.88)[8-10]; however, clinically, only 30%-66% of PAS pregnancies are diagnosed before birth.[11-13] Furthermore, approximately 50% of PAS mothers also exhibit placenta previa (PP), where the placenta partially or completely covers the cervix (without abnormal placental attachment).[4,14] It is important to accurately distinguish healthy placenta, PP (without PAS) and PAS, as the conditions have different risks and require different management strategies.

Texture analysis is the quantification of the pattern of grey values on an MRI.[6,15,16] It has been utilized to quantify MRI indications of PAS, with areas under the receiver operating characteristic curve (AUCs) of 0.64-0.82 reported for classification of PAS and healthy placentas using MRI-derived texture features.[1,14,17,18] However, there has been no investigation of the optimal anatomical plane for manual placental segmentation with regards to segmentation repeatability, which acts as a crucial benchmark for follow-up quantitative analyses. Ren et al[2]

Received: October 16, 2025. **Revised:** May 8, 2026. **Accepted:** August 10, 2026
© The Author(s) 2026. Published by Oxford University Press on behalf of the British Institute of Radiology.
This is an Open Access article distributed under the terms of the Creative Commons Attribution License (https://creativecommons.org/licenses/by/4.0/), which permits unrestricted reuse, distribution, and reproduction in any medium, provided the original work is properly cited.

Downloaded from academic.oup.com/bjr/advance-article/doi/10.1093/bjr/tqag194/8767767 by guest on 30 September 2026

demonstrated that texture features derived from the coronal and sagittal planes achieved the highest AUCs (0.85-0.97) for classifying PAS. In contrast, Do et al[19] reported AUCs of 0.79 and 0.72 in the axial and sagittal planes for the prediction of PPH. Neither study reported segmentation repeatability.

Few studies have investigated the effect of gestational age (GA) on texture and shape features of the placenta, even though the placenta is known to adapt to accommodate the growing fetus, increasing in volume and heterogeneity throughout pregnancy.[15,20] Chen et al[21] are the only authors to establish associations with GA in PAS; however, they investigated less commonly utilized texture features, such as histogram oriented gradients, making results hard to compare. Andescavage et al[22] and Sun et al[23] studied correlation of texture features with GA in healthy and PP cohorts respectively. Both studies reported grey level non-uniformity (GLNU) and run length non-uniformity to be significantly associated with GA. On the other hand, a third study by Do et al,[15] demonstrated that correlation and entropy were significantly correlated with GA in healthy placentas, contradicting Sun et al.[23] It is worth noting that all 3 studies investigated different numbers of features (6, 13, and 624 respectively) calculated using different software (in-house MATLAB pipeline, PyRadiomics, and pyOsirix, respectively), which may explain the discrepancies in their results.

To date, there is no definitive consensus on the most repeatable anatomical plane for placental segmentation in MRI. It is also challenging to quantify the change in texture and shape features throughout gestation and compare these changes across healthy placentas, PP, and PAS, based on the scarce literature. Therefore, the aims of this study are to: (1) determine the most repeatable anatomical plane for manual whole placental segmentation of healthy placenta and PAS and (2) investigate potential correlation between GA and texture and shape features extracted from healthy placenta, PP and PAS MRI using PyRadiomics, a publicly available software with full documentation developed in line with the Imaging Biomarker Standardization Initiative.[24]

Methods

Patients

MRIs from healthy volunteers were collected from a previous research project. Exclusion criteria were placental anomalies (fetal growth restriction (FGR), small for GA, twin-to-twin transfusion syndrome), PAS indications on MRI or during birth and PP. Sixty-three patients (65 pregnancies; 2 patients had multiple pregnancies) were recruited and had MRIs in the second and third trimesters. In eighteen pregnancies, there were 2 MRIs and in 1 pregnancy there were 3 MRIs.

MRIs from PAS suspected patients were collected from clinical diagnosis; these were split into 2 groups: PAS and PP. Inclusion criteria for PAS was routine histological assessment at an NHS hospital verifying the presence of PAS and its subtype (accreta, increta, or percreta). Inclusion criteria for PP was imaging demonstrating the placenta covering or within 2 cm of the internal os and a complete placenta at delivery. A total of 123 participants were recruited; 4 participants had 2 MRIs during the same pregnancy.

MRI protocol

All placental MRIs were obtained on 1.5 T scanners (Siemens Advent or Siemens Aera, Siemens Healthcare). The same protocol was used, which included sagittal, axial, and coronal T2 single shot fast spin echo scans (TE = 90 ms, TR = 1000 ms). Healthy MRIs had an in-plane resolution of 1.5-1.8 mm and a slice thickness of 4-4.5 mm; PAS suspected MRIs exhibited an in-plane resolution of 0.5-1.8 mm and a slice thickness of 3-9 mm. The variations in image resolution and slice thickness are a result of scanner adaptation to patient body habitus and placental volume, the latter of which is higher in PP and PAS, pointing to the higher variations seen in these MRIs compared with the healthy cases. Since these were clinical scans to a set proforma there will inevitably be heterogeneity in the image dimensions due to scanner and patient variables.

Segmentation

A conservative segmentation guideline was used:

1) The whole placenta was segmented.
2) The placental boundary was avoided.
3) If available, a sagittal diffusion-weighted imaging MRI was utilized to ascertain placental shape.
4) Slices with <1000 mm^2 (ellipsoid area) of placenta were not segmented.
5) Slices with no defined placental boundary were not segmented.

Figure 1 illustrates representative segmentations in each anatomical plane. Segmentation was conducted in ITK-Snap (version 4.0.2) by 3 operators and reviewed by a Consultant Radiologist with >20 years' experience in placenta-fetal MRI diagnosis.

Texture and shape analysis

Texture and shape features were extracted from each MRI using PyRadiomics (version 3.0.1).[25] Pre-processing included normalization and image filtering with the wavelet, exponential, local binary pattern 3D (LBP3D), and Laplacian of Gaussian methods, chosen as visual examination identified that they highlighted placental texture. A total of 93 texture features were extracted in 2D and 3D for the original, wavelet, exponential and Laplacian of Gaussian images, but only in 3D for the LBP3D images. Fourteen shape features were extracted in 3D from the original MRI. Specific parameters and feature classes are shown in Table 1.

Intra- and inter-observer segmentation study

Segmentation repeatability was investigated with 3 PAS (1 of each subtype: accreta, increta, and percreta) and 3 healthy placentas. PP were not used in the segmentation study due to their similar morphology to PAS. For each placenta, the sagittal, axial and coronal MRIs were segmented 3 times by 3 independent operators (I-III) who were provided with the segmentation guideline; segmentations were not reviewed by the Consultant Radiologist for this study. As far as the authors are aware, this segmentation study used more repeats per operator and more

Downloaded from academic.oup.com/bjr/advance-article/doi/10.1093/bjr/tqag194/8767767 by guest on 30 September 2026

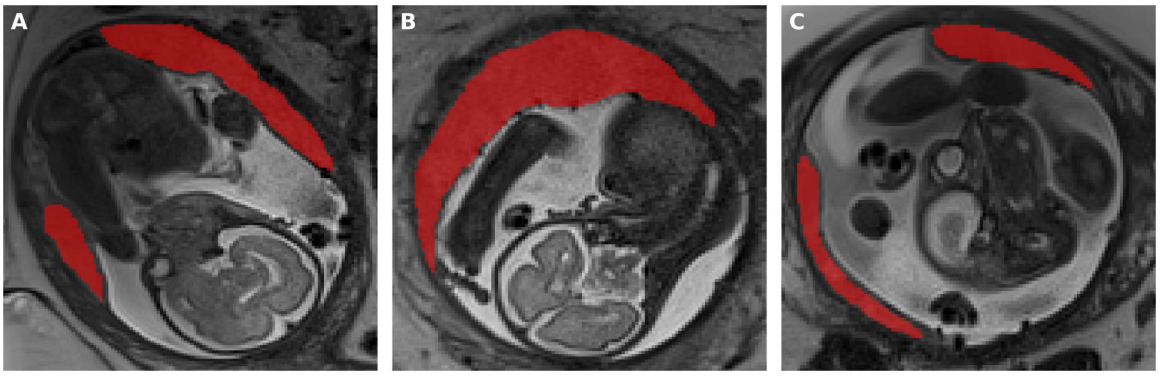


Figure 1 T2 MRI of the placenta of a healthy subject (32 weeks) in the (A) sagittal, (B) coronal, and (C) axial anatomical planes. The segmented placenta is highlighted in red.

Table 1 Input parameters for pre-processing, image filtering, feature classes, and the extraction types used in PyRadiomics.[a]

Process	Input parameters
Pre-processing	
Normalization	"NormalizeScale" of 100, bin count of 128 following methodology in Koçak et al[26] and Duron et al[27]
Wavelet	"level" 1, "start_level" 0, and "wavelet" types were "bior1.1," "coif1," "dmey," and "sym2"; outputs LL/LLL and LH/LLH.
Exponential	n/a
Local binary pattern 3D (LBP3D)	"lbp3DLevels" 2, "lbp3DIcosphereRadius" 1, and "lbp3DIcosphereSubdivision" 2; m1, m2, and k outputs.
Laplacian of Gaussian	"Sigma" of 1 and 2.
Feature Classes	
First order	"VoxelArrayShift" of 300.
Grey level co-occurrence matrix (GLCM)	n/a
Grey level run length matrix (GLRLM)	n/a
Grey level size zone matrix (GLSZM)	n/a
Neighboring grey tone difference matrix (NGTDM)	n/a
Grey level dependence matrix (GLDM)	n/a
Feature extraction	
2D	"force2D" True, "force2Ddimension" of 0.
3D	"force2D" False.

[a]Filters and their specific parameters were chosen as visual examination identified that they highlighted placental texture. All other parameters in PyRadiomics were set to default values.

operators than previous literature, which has mainly investigated 1 repeat with only 2 other operators.[1,28-30]

The dice coefficient (DC) and Hausdorff distance (HD) were used to determine repeatability of segmented volumes,[31,32] using 3D Slicer (version 5.6.0). The 95th centile HD was used to exclude outliers, as segmented volumes often exhibit protruding edges. The intraclass correlation coefficient (ICC) (2-way mixed single measure), was used to determine the repeatability of texture and shape features derived from each segmentation.

For the intra-observer study, the DC, HD, and ICC were calculated by comparing the segmentation from operator I in each anatomical plane. For the inter-observer study, this was extended to include the repeats from operators II and III. Normality was evaluated using the Anderson Darling and Shapiro-Wilk test; Kruskal-Wallis and Dunn's tests were used to determine any significant differences in DC, HD, and ICC between the anatomical planes for healthy and PAS.

Correlation with GA

PAS, PP, and healthy sagittal MRIs were used to investigate the correlation, following the segmentation study outcome. For cases with more than 1 MRI in pregnancy (longitudinal data), only 1 MRI was used for the correlation analysis, to avoid introducing any bias into the statistics. Features with an ICC < 0.75 from the segmentation study were excluded; feature normality was evaluated using the Anderson Darling and Shapiro-Wilk test. Absolute Spearman's correlation coefficient (ρ) was used to determine any monotonic relationship between each feature and GA (strong: $\rho > 0.7$, moderate: $0.4 < \rho < 0.7$, and weak: $\rho < 0.4$). A permutation test was performed to indicate the significance of the correlation. Linear and polynomial regressions (degree = 2) were conducted with the ordinary least squares method. Analysis was executed in Python (version 3.11.5), with $P < .05$ for significance.

Downloaded from academic.oup.com/bjr/advance-article/doi/10.1093/bjr/tqag194/8767767 by guest on 30 September 2026

Results

Patient characteristics

Patient characteristics and MRI information for the segmentation study are shown in Table 2. A range of image resolutions were chosen such that segmentation results would represent clinical MRIs with different image dimensions. The selection of healthy, PAS, and PP placentas for the correlation study is shown in Figure 2. The final number of pregnancies included for healthy, PAS, and PP was 46, 49, and 57, respectively. Patient characteristics can be found in Table 3.

Intra-observer segmentation study

For healthy placentas, the coronal plane exhibited the highest median DC (0.935) and lowest median HD (4.0 mm), closely followed by the sagittal plane (0.925 and 4.2 mm) (Figure 3A and B). The axial plane had the lowest median DC (0.918) and highest median HD (6.0 mm), along with the largest interquartile range (IQR) for both metrics.

For PAS cases, the sagittal plane exhibited the highest median DC (0.915), although there was little difference between the 3 anatomical planes. The sagittal plane exhibited the lowest median HD (4.5 mm), followed by the axial (5.1 mm) and coronal (6.0 mm). The PAS cases demonstrated worse median and IQR of the DC and HD in the sagittal and coronal planes than the healthy cases.

All anatomical planes exhibited a similar percentage of texture and shape features with ICC $>$ 0.750 (Table 4). Despite similar median ICCs, there was a significant difference between each anatomical plane ($P < .001$).

Inter-observer segmentation study

The sagittal plane exhibited the highest median DC (healthy: 0.907, PAS: 0.891) and lowest median HD (healthy: 4.62 mm, PAS: 6.25 mm), along with the smallest IQR for both metrics (Figure 3C and D).

The sagittal and axial planes exhibited similarly high ICC (Table 4). There was a statistically significant difference in the

Table 2 Patient characteristics and image information for the segmentation study.

Patient	Condition	Maternal age (years)	Gestational age (weeks)	In-plane image resolution (mm)			Slice thickness (mm)		
				Sag	Cor	Ax	Sag	Cor	Ax
1	Healthy	30	22	1.5	1.5	1.5	4	4	4
2	Healthy	32	32	1.5	1.5	1.5	4	4	4
3	Healthy	42	36	1.5	1.5	1.5	4.5	4	4
4	Accreta	35	32	1.5	1.5	1.5	4	4	4
5	Increta	23	35	0.7	0.7	0.7	3.3	3	3
6	Percreta	33	32	1.5	1.5	1.5	4	4	4.5

Abbreviations: ax = axial, cor = coronal, sag = sagittal.

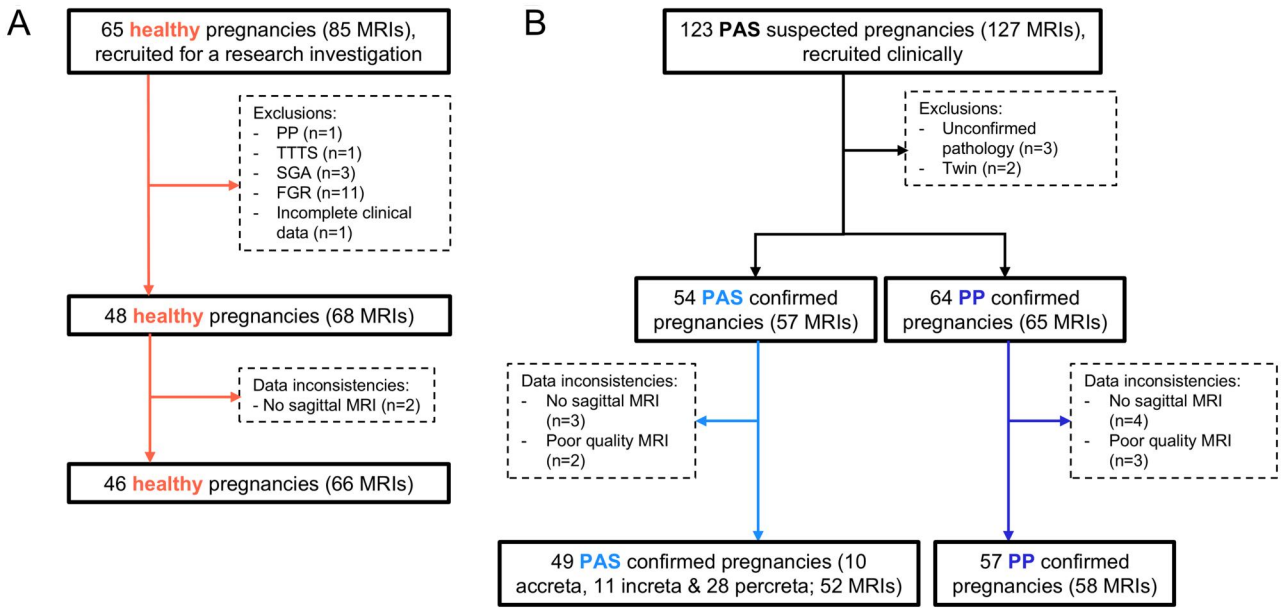


Figure 2 Flowchart of the exclusion criteria for (A) healthy and (B) PAS suspected participants. Abbreviations: FGR, fetal growth restriction; *n*, indicates the number of pregnancies excluded; PAS, placenta accreta spectrum; PP, placenta previa; SGA, small for gestational age; TTTS, twin-to-twin transfusion syndrome.

Downloaded from academic.oup.com/bjr/advance-article/doi/10.1093/bjr/tqag194/8767767 by guest on 30 September 2026

Table 3 Demographic characteristics of the final participant groups.[b]

Characteristic[a]	Healthy group ($m = 46$, $n = 66$)	PAS group ($m = 49$, $n = 52$)	PP group ($m = 57$, $n = 58$)
Gestational age (weeks)	27 ± 5.2 (19-38)	30 ± 3.8 (20-38)	31 ± 3.4 (21-37)
Maternal age (years)	33 ± 4.7 (22-42)	33 ± 5.0 (21-43)	33 ± 4.3 (22-42)
Number of scans	1.4 ± 0.54 (0-3)	1.1 ± 0.2 (1-2)	1.0 ± 0.1 (1-2)
Parity	0.82 ± 0.94 (0-5)	2.1 ± 1.2 (1-7)	1.7 ± 1.2 (0-7)
Race and ethnicity			
White British	26	23	20
White Other	2	2	3
Chinese	1	0	0
Iran-German	1	0	0
Czechia (Slovakia)	1	0	0
Iranian	1	0	0
Pakistani	0	1	5
Bangladeshi	0	1	0
African	0	3	2
Asian	0	3	0
Mixed other	0	2	0
Not reported	15	14	27
Maternal weight (kg)	74 ± 16 (54-123)	79 ± 18 (47-139)	75 ± 12 (43-105)
Percentage of cases of PP minor (%)	0	2	37
Percentage of cases with PP major (%)	0	88	63

[a]1 healthy, 1 PAS, and 1 PP pregnancies were missing maternal age; 8 healthy, 5 PAS, and 15 PP pregnancies were missing parity.
[b]Information is reported as mean ± SD (range) to 2 significant figures. *m* indicates number of pregnancies and *n* indicates number of MRIs.

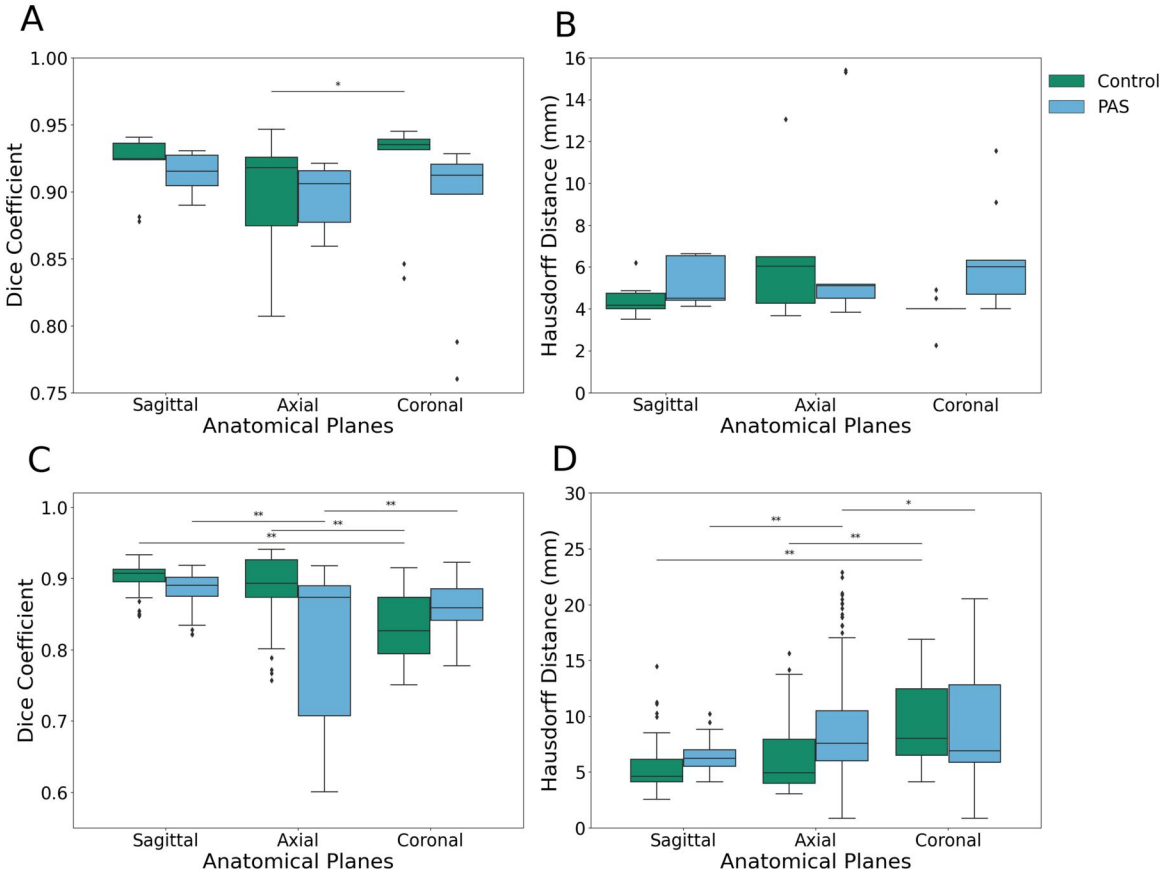


Figure 3 Intra-observer (A, B) and inter-observer (C, D) segmentation study; DC (A, C) and 95th centile HD (B, D) for each anatomical plane and each participant group (healthy in green, PAS in blue). $N = 9$ for each box in the intra-observer study and $n = 27$ for each box in the inter-observer study. *$P < .05$ and **$P < .001$ for statistically significant difference between groups. Abbreviations: DC, dice coefficient; HD, Hausdorff distance.

Downloaded from academic.oup.com/bjr/advance-article/doi/10.1093/bjr/tqag194/8767767 by guest on 30 September 2026

median ICC between all anatomical planes ($P < .001$ for sagittal and coronal, and axial and coronal; $P < .05$ for axial and sagittal).

Correlation with GA

A total of 2525 features were extracted from each MRI. Only 29 were parametric, so for consistency all were treated as non-parametric. Due to ICC < 0.750 reported in the segmentation study, 532 features were excluded.

Twelve texture and 4 shape features displayed a strong and significant correlation with GA ($\rho > 0.70$, $P < .001$) in the healthy group (Table 5). However, no texture or shape features exhibited a strong correlation ($\rho > 0.70$) in the PAS or PP groups. Sixty-four texture and 7 shape features showed a moderate correlation ($\rho > 0.40$, $P < .01$) in the PP group, and 70 texture and 7 shape features showed a moderate correlation ($\rho > 0.40$, $P < .01$) in the PAS group. Some of these features were also strongly correlated in the healthy group (eg, busyness, strength and coarseness; Table 5). Most (80%) features which displayed $\rho > 0.40$ in the PP and PAS groups, also displayed $\rho > 0.40$ in the healthy group.

Many of the texture features with a strong ρ in the healthy group highlighted non-uniformities of the placenta (Table 5). Grey level non-uniformity derived from the same LBP3D filter is plotted against GA in Figure 4 for the healthy, PP, and PAS groups. For healthy subjects, GLNU increased with GA ($\rho = 0.81$, $P < .001$), highlighted by the reasonable linear regression ($R^2 = 0.58$). This increase is further confirmed in Figure 4B, which

Table 4 Intraclass correlation coefficient for the intra- and inter-observer studies.[a]

Anatomical Plane	Intra-observer		Inter-observer	
	Median ICC	Percentage ICC > 0.75 (%)	Median ICC	Percentage ICC > 0.75 (%)
Sagittal	0.98 ± 0.07	94	0.97 ± 0.12	87
Axial	0.99 ± 0.04	99	0.96 ± 0.10	93
Coronal	0.98 ± 0.05	95	0.94 ± 0.15	81

Abbreviation: ICC = intraclass correlation coefficient.
[a]Median ICC (±interquartile range) and the percentage of texture and shape features with an ICC > 0.75 are included.

Table 5 Texture and shape features with the highest Spearman's correlation coefficients (ρ) in the healthy, PP, and PAS groups.[a]

Feature		Highest associated ρ			Number of image filters where $\rho > 0.7$ (healthy) or $\rho > 0.4$ (PP/PAS)		
		Healthy	PP	PAS	Healthy	PP	PAS
Features with the highest correlation coefficients in the healthy group							
Texture	Strength	−0.79***	−0.58***	−0.53***	2	22	17
	GLNU	0.81***	0.58***	0.52***	18	80	77
	RLNU	0.74***	0.50***	0.50***	24	25	24
	SZNU	0.75***	0.50***	0.50**	18	22	16
	Coarseness	−0.72***	0.57***	−0.52**	13	25	21
	DNU	0.76***	0.55***	0.51***	21	27	27
	Busyness	0.75***	0.67***	0.55***	3	22	25
	LALGLE	0.76***	0.53***	0.48***	1	5	4
Shape	Surface Area	0.79***	0.43***	0.56***	n/a	n/a	n/a
	Minor axis length	0.75***	0.40**	0.52***	n/a	n/a	n/a
	Voxel volume	0.74***	0.46***	0.46**	n/a	n/a	n/a
	Mesh volume	0.74***	0.46***	0.46**	n/a	n/a	n/a
Features with the highest correlation coefficients in the PP or PAS groups							
Texture	Busyness	0.75***	0.67***	0.55***	3	22	25
	HGLRE	−0.61***	−0.61***	−0.54***	n/a	4	2
	Cluster shade	−0.65***	−0.44**	0.65***	n/a	1	11
	Skewness	−0.44**	0.39**	0.69***	n/a	n/a	11
Shape	Major axis length	0.56***	0.43**	0.57***	n/a	n/a	n/a
	Surface area	0.79***	0.43**	0.56***	n/a	n/a	n/a

*$P < .05$. **$P < .01$. ***$P < .001$.
Abbreviations : DNU = dependence non-uniformity; GLNU = grey level non-uniformity; HGLRE = high grey level run emphasis; LALGLE = large area low grey level emphasis; RLNU = run length non-uniformity; SZNU = size zone non-uniformity; ρ = absolute Spearman's correlation coefficient.
[a]The table shows the highest ρ displayed by each feature across different image filters for each group (columns 3-5). Positive/negative indicates increasing/decreasing with GA. In addition, the number of times this feature exhibited a strong correlation ($\rho > 0.7$) in the healthy cohort or moderate correlation ($\rho > 0.4$) in the PP/PAS cohort across different image filters (columns 6-8).

Downloaded from academic.oup.com/bjr/advance-article/doi/10.1093/bjr/tqag194/8767767 by guest on 30 September 2026

shows 19 healthy cases with 2/3 MRIs during pregnancy with varying slope for different individuals. These changes are highlighted visually on MRIs in Figure 5. The PP and PAS groups also exhibited an increase in GLNU with GA (Figure 4), with much larger absolute values and steeper slopes but weaker correlations and poorer linear regressions (PP: $\rho = 0.52$, $R^2 = 0.10$, $P < .001$; PAS: $\rho = 0.52$, $R^2 = 0.23$, $P < .001$).

In the PP group, busyness exhibited the highest correlation coefficient ($\rho = 0.67$, $P < .001$). Busyness was strongly correlated in the healthy group ($\rho = 0.75$, $P < .001$) and moderately correlated in the PAS group ($\rho = 0.55$, $P < .001$; Table 5). In the PAS group, skewness exhibited the highest correlation coefficient, demonstrating a moderate to strong correlation with GA ($\rho = 0.69$, $P < .001$). In contrast, skewness displayed a moderate and weak correlation in the healthy and PP groups ($\rho = 0.44$ and 0.39, respectively, $P < .01$ for both).

Surface area exhibited a strong and moderate correlation in the healthy and PAS groups ($\rho = 0.79$ and 0.56, respectively, $P < .001$ for both) (Figure 6). In addition, most PAS and some PP cases exhibited a larger surface area than healthy placentas at the same GA; this is highlighted visually in Figure 5. In the PP group, mesh and voxel volume exhibited the highest corelation coefficient amongst other shape features ($\rho = 0.46$, $P < .001$); mesh and voxel volume exhibited a strong and moderate correlation in the healthy and PAS group (healthy: $\rho = 0.74$, $P < .001$; PAS: $\rho = 0.46$, $P < .01$).

The magnitude of the correlation coefficient of the texture features extracted in 3D for the healthy group is displayed for each image filter in Figure 7. Some features were strongly correlated with GA across many filters, eg, energy and total energy (first order) and GLNU (GLRLM, GLSZM, and GLDM). The same trend was also exhibited for 2D extraction but is not shown here.

Discussion

We investigated the repeatability of 3 anatomical planes for manual placental segmentation and the correlation of texture and shape features with GA. The sagittal plane exhibited the best overall DC, HD, and ICC, as it was the easiest anatomical plane to delineate the placental-fetal and placental-

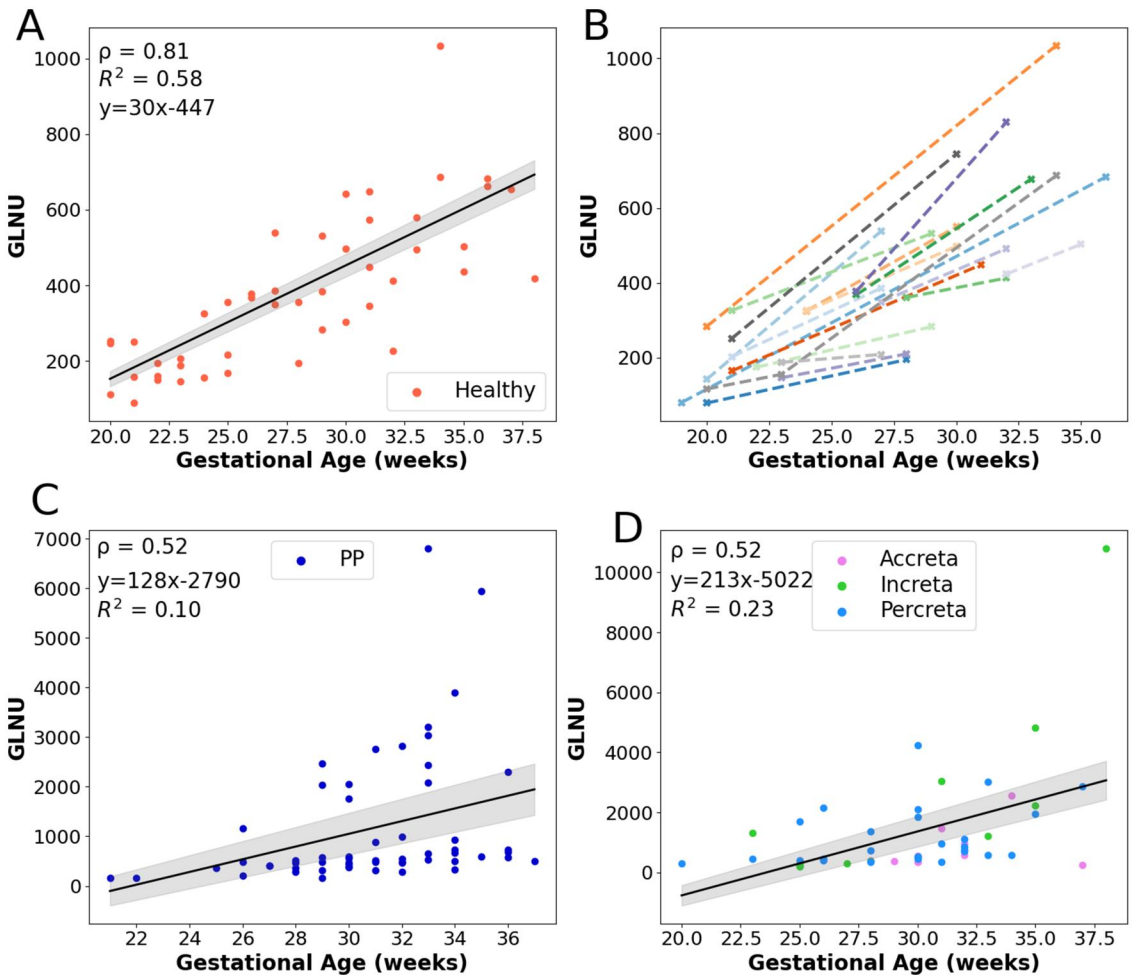


Figure 4 Grey level non-uniformity across gestation for the healthy (A, B), PP (C), and PAS (D) participants. (A, C, D) Changes across gestation with 1MRI per pregnancy, with a linear regression line (black) and 95% CIs (grey shaded area); linear regression was chosen over polynomial regression due to the better R^2. (B) Changes across longitudinal scans at different time points, with each participant shown as a different color. (D) PAS subtypes are shown as accreta in pink, increta in green, and percreta in blue. For consistency, GLNU was derived from the GLSZM in a 3D manner using the LBP3D filter (kurtosis output) for all groups.

Downloaded from academic.oup.com/bjr/advance-article/doi/10.1093/bjr/tqag194/8767767 by guest on 30 September 2026

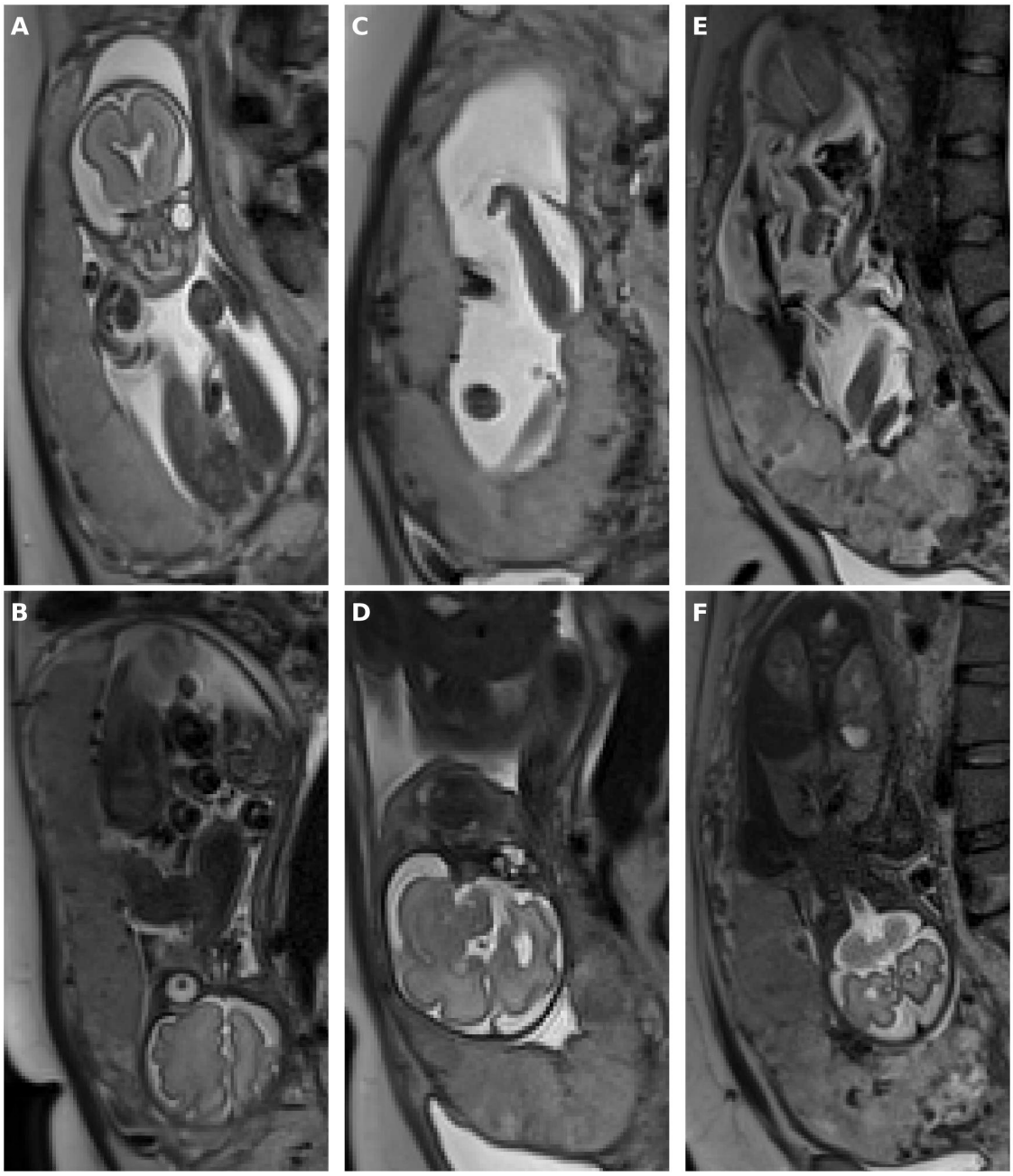


Figure 5 T2 MRIs of (A, B) healthy, (C, D) PP, and (E, F) PAS placentas. (A, B) the same healthy placenta at 21 weeks (A) and 30 weeks (B) gestation showing increased heterogeneity within its structure toward later stage of pregnancy. This individual is represented by the dark grey line in the longitudinal scan plots in Figures 4 and 6. (C, D) Two different placentas with PP at 21 weeks (C) and 30 weeks (D), both with PP major. Both placentas appear larger than the healthy placentas and display a slight increase in heterogeneity toward later gestation. (E, F) Two different placentas with PAS (percreta with PP major) at 23 weeks (E) and 32 weeks (F). The presence of PAS can be seen, along with the larger size of the placenta. All MRIs have an in-plane image resolution of approximately 1.5 mm, and a slice thickness of approximately 4 mm.

endometrium boundaries. The axial plane contained thinner regions of placenta (Figure 1), leading to more data loss. In the coronal plane, the placenta was more frequently obstructed by maternal and fetal tissues, resulting in volume averaging (Figure 1).

Texture features with a strong correlation with GA in healthy placentas were indicators of non-uniformities, heterogeneity, and grey value magnitude. For example, GLNU indicates the variability of grey values.[25] Through gestation, the placenta becomes more vascular to increase the oxygen and nutrient supply to the growing fetus. In addition, maturation of the placenta's functional units involves increased fibrin deposition and calcification, which can contribute to a more granulated appearance (Figure 5).[15,20] For PP and PAS, texture features exhibited weak to moderate correlations with GA, indicating that abnormalities associated with PAS and PP may mimic changes of GA

Downloaded from academic.oup.com/bjr/advance-article/doi/10.1093/bjr/tqag194/8767767 by guest on 30 September 2026

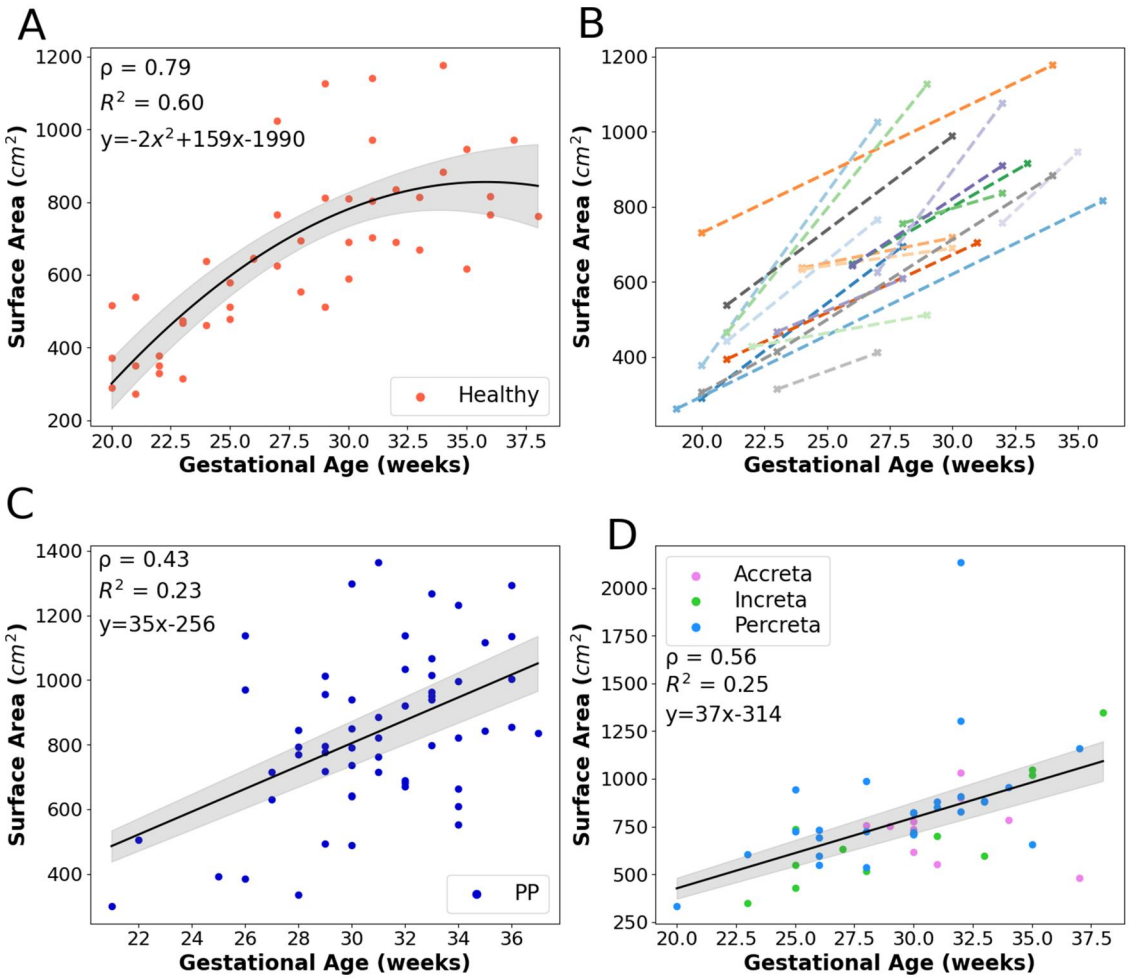


Figure 6 Surface area (cm^2) across gestational age for the healthy (A, B), PP (C), and PAS (D) participants. (A, C, D) Changes across gestation with 1MRI per pregnancy, with a polynomial or linear regression line (black) and 95% CIs (grey shaded area); the regression type with the highest R^2 was chosen for each group. (B) Changes across longitudinal scans at different time points, with each participant shown as a different color. (D) PAS subtypes are shown as accreta in pink, increta in green, and percreta in blue.

and occur earlier in pregnancy. Skewness exhibited the highest correlation coefficient in the PAS group, with a higher correlation coefficient than the healthy and PP groups, indicating that later in gestation more grey values exhibited a lower signal intensity on PAS MRIs, which was not as prominent on healthy and PP MRIs (ie, darker on MRI; Figure 5).[25] This is in agreement with PAS being associated with abnormal placental vascularity and exhibiting indications such as dark intraplacental bands on T2 MRI (Figure 5).[2,3,7,21,33] Busyness exhibited the highest correlation coefficient in the PP group, indicating that later in GA there were increasingly rapid intensity changes between voxels.[25]

Regarding shape features, healthy placentas exhibited a strong correlation with surface area and volume, highlighting the increase in size of the placenta. The PP group exhibited the lowest correlation coefficients associated with shape features, compared with the healthy and PAS groups, indicating that the PP group showed the least amount of placental shape variations across GA. In the PAS group, surface area exhibited a weaker correlation (0.56) than healthy (0.79). However, PAS generally exhibited a larger surface area than healthy placentas (Figures 5 and 6), implying that shape changes occurring because of PAS may have started early in pregnancy and continued with increasing GA.

We reported a median DC for the intra- and inter-observer studies in line with previous literature (0.82-0.98 and 0.79-0.995, respectively) which investigated healthy, PAS and FGR placentas.[1,28,29] The median ICC is slightly higher than those reported in the literature (0.86 and 0.878-0.95, respectively, for intra- and inter-observer studies).[30,34,35]

The significant increase in GLNU and run length non-uniformity throughout gestation in healthy placenta (Table 5) concurs with Andescavage et al,[16,22] although our study found values lower than the 10th centiles reported in Andescavage et al,[22] particularly earlier in gestation. Our findings are further supported by Sun et al,[23] who reported that GLNU, run length non-uniformity, dependence non-uniformity, and coarseness were significantly affected by GA in PP. Sun et al[23] modeled the effect of GA with linear drift, but the R^2 values reported here indicate this method may require further refinement, particularly

Downloaded from academic.oup.com/bjr/advance-article/doi/10.1093/bjr/tqag194/8767767 by guest on 30 September 2026

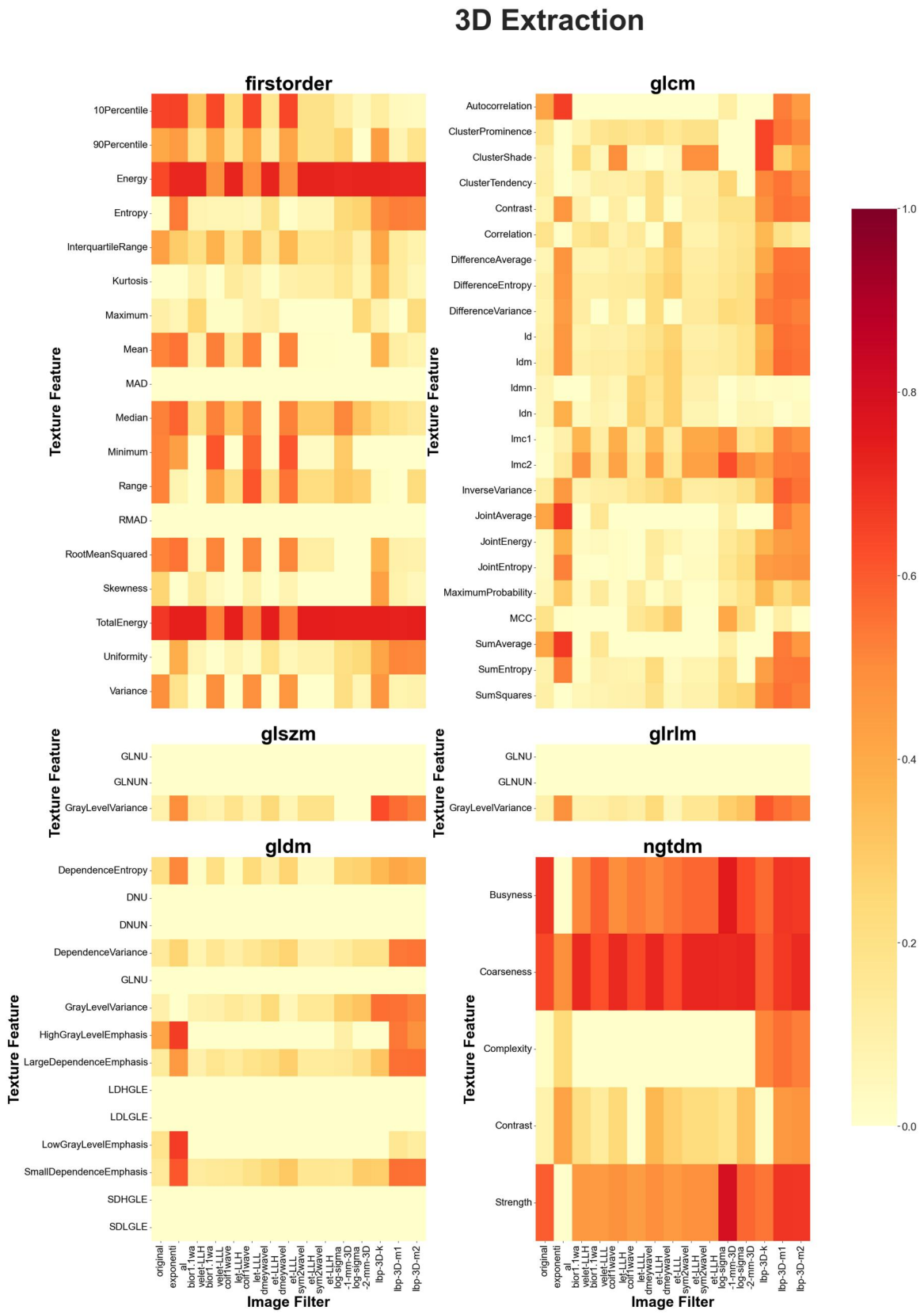


Figure 7 Heatmaps displaying the absolute Spearman's correlation coefficient for each texture feature with ICC > 0.75 (y axis) and each image filter (x axis), from each of the feature classes for the 3D extraction from the healthy group. Red indicates a high ρ and yellow indicates a low ρ. Abbreviations: DNUN, dependence non-uniformity normalized; DNU, dependence non-uniformity; LDHGLE, large dependence high grey level emphasis; LDLGLE, large dependence low grey level emphasis; GLCM, grey level co-occurrence matrix; GLDM, grey level dependence matrix, GLNUN, grey level non-uniformity normalized; GLNU, grey level non-uniformity; GLRLM, grey level run length matrix; GLSZM, grey level size zone matrix; MAD, mean absolute deviation; NGTDM, neighboring grey tone difference matrix; RMAD, robust mean absolute deviation; SDHGLE, small dependence high grey level emphasis; SDLGLE, small dependence low grey level emphasis.

Downloaded from academic.oup.com/bjr/advance-article/doi/10.1093/bjr/tqag194/8767767 by guest on 30 September 2026

for PP and PAS groups. In contrast to Do et al,[15] this study did not find significant correlations between GA and sum of squares or sum entropy in the healthy group.

Concerning shape features, both our study and previous literature have shown a significant correlation between placental volume and GA in healthy placenta, with Do et al[15] reporting a lower correlation coefficient (ρ = 0.62) compared to the current study (ρ = 0.74). Similar to texture features, 54% of placental volumes in the current study were below the 10th centiles reported in Andescavage et al.[22] In addition, Andescavage et al[22] described a significant increase in elongation, which was not found in the current study (ρ = 0.25, $P > .05$). This could be attributed to numerous factors including sample size, different anatomical planes used for segmentation and the conservative segmentation approach used in this study resulting in a lower overall placental volume.

This study has several limitations. Firstly, the spread of GA was different across the 3 groups. Future improvements could be made by including more PP and PAS MRIs at 20-25 weeks gestation, more accreta and increta PAS subtypes and more longitudinal PP and PAS cases. Secondly, as seen in Figures 4 and 6, numerous data points fell outside of the 95% CI of the linear and polynomial regressions in all patient groups. This is likely due to the heterogeneous development of the placenta and intra-personal variations, pointing to the need for a larger group to ascertain the current findings. Thirdly, the image resolution and slice thickness varied across MRIs, particularly in the PP and PAS groups. The inconsistent image dimensions may have contributed to the weaker correlations and increased heterogeneity exhibited by PP and PAS MRIs. A higher image resolution would allow for better depiction of placental texture; however, this would increase the scan duration, and hence the risk of fetal motion artifacts and cost. Considering that the segmentation method must be robust to real life clinical data collected at different centers, with varying image dimensions (eg, previously reported image resolutions: 0.77-2.15 mm and slice thicknesses: 4-7mm.[1,17,18,35-37]), the use of heterogeneous image dimensions could be considered a strength of this study. The results highlighted that accurate segmentation can still be achieved using the sagittal plane, illustrating the potential usefulness of texture and shape analysis in multi-center clinical data. All these factors need to be considered to achieve a balanced decision between image quality, scan time and resource requirement. A future study will also be conducted to quantify the variations exhibited by texture and shape features derived from MRIs with heterogeneous image dimensions. Finally, GA itself was an estimation based on the date of the last menstrual cycle and fetal measurements derived from a 12-week ultrasound scan. Therefore, the values of GA used also carried a small margin of error.

In conclusion, to the authors' knowledge this is the first study to systematically demonstrate that the sagittal plane is the most repeatable anatomical plane for manually segmenting healthy placentas and PAS using MRI. We have also reported quantitative texture and shape changes in the placenta during gestation in healthy, PP, and PAS in a UK-based population, using texture features derived from PyRadiomics. Many texture and shape features exhibited a strong correlation with GA in the healthy group, whilst some showed a moderate correlation in the PP and PAS groups. This indicates a need to potentially consider texture and shape changes due to GA when classifying healthy, PP, and PAS.

Conflicts of interest

The authors have no conflicts of interest to declare.

Funding

This study has received funding from the Insigneo Institute for Healthcare Technology and the EPSRC.

References

1. Peng L, Zhang X, Liu J, et al. MRI–radiomics–clinical–based nomogram for prenatal prediction of the placenta accreta spectrum disorders. *Eur Radiol*. 2022;32:7532-7543. https://doi.org/10.1007/s00330-022-08821-4
2. Ren H, Mori N, Mugikura S, et al. Prediction of placenta accreta spectrum using texture analysis on coronal and sagittal T2-weighted imaging. *Abdom Radiol (NY)*. 2021;46:5344-5352. https://doi.org/10.1007/s00261-021-03226-1
3. Morlando M, Collins S. Placenta accreta spectrum disorders: challenges, risks, and management strategies. *Int J Womens Health*. 2020;12:1033-1045. https://doi.org/10.2147/ijwh.S224191
4. Lu T, Zhang T, Wang Y, et al. Radiomics analysis of T(2)-weighted images for differentiating invasive placentas in women at high risks. *Magn Reson Med*. 2022;88:2621-2632. https://doi.org/10.1002/mrm.29396
5. Do Q, Lewis M, Xi Y, et al. MRI of the placenta accreta spectrum (PAS) disorder: radiomics analysis correlates with surgical and pathological outcome. *J Magn Reson Imaging*. 2020;51:936-946. https://doi.org/10.1002/jmri.26883
6. Wu Q, Yao K, Liu Z, et al. Radiomics analysis of placenta on T2WI facilitates prediction of postpartum haemorrhage: a multicentre study. *EBioMedicine*. 2019;50:355-365. https://doi.org/10.1016/j.ebiom.2019.11.010
7. Jha P, Põder L, Bourgioti C, et al. Society of Abdominal Radiology (SAR) and European Society of Urogenital Radiology (ESUR) joint consensus statement for MR imaging of placenta accreta spectrum disorders. *Eur Radiol*. 2020;30:2604-2615. https://doi.org/10.1007/s00330-019-06617-7
8. De Oliveira Carniello M, Oliveira Brito LG, Sarian LO, Bennini JR. Diagnosis of placenta accreta spectrum in high-risk women using ultrasonography or magnetic resonance imaging: systematic review and meta-analysis. *Ultrasound Obstet Gynecol*. 2022;59:428-436. https://doi.org/10.1002/uog.24861
9. Hong S, Le Y, Lio KU, Zhang T, Zhang Y, Zhang N. Performance comparison of ultrasonography and magnetic resonance imaging in their diagnostic accuracy of placenta accreta spectrum disorders: a systematic review and meta-analysis. *Insights Imaging*. 2022;13:50. https://doi.org/10.1186/s13244-022-01192-w
10. Meng X, Xie L, Song W. Comparing the diagnostic value of ultrasound and magnetic resonance imaging for placenta

Downloaded from academic.oup.com/bjr/advance-article/doi/10.1093/bjr/tqag194/8767767 by guest on 30 September 2026

accreta: a systematic review and meta-analysis. *Ultrasound Med Biol*. 2013;39:1958-1965. https://doi.org/10.1016/j.ultrasmedbio.2013.05.017
11. McCall SJ, Deneux-Tharaux C, Sentilhes L, et al. Placenta accreta spectrum–variations in clinical practice and maternal morbidity between the UK and France: a population-based comparative study. *BJOG*. 2022;129:1676-1685. https://doi.org/10.1111/1471-0528.17169
12. Fitzpatrick KE, Sellers S, Spark P, Kurinczuk JJ, Brocklehurst P, Knight M. The management and outcomes of placenta accreta, increta, and percreta in the UK: a population-based descriptive study. *BJOG*. 2014;121:62-70. https://doi.org/10.1111/1471-0528.12405
13. Thurn L, Lindqvist PG, Jakobsson M, et al. Abnormally invasive placenta—prevalence, risk factors and antenatal suspicion: results from a large population-based pregnancy cohort study in the nordic countries. *BJOG*. 2016;123:1348-1355. https://doi.org/10.1111/1471-0528.13547
14. Romeo V, Ricciardi C, Cuocolo R, et al. Machine learning analysis of MRI-derived texture features to predict placenta accreta spectrum in patients with placenta previa. *Magn Reson Imaging*. 2019;64:71-76. https://doi.org/10.1016/j.mri.2019.05.017
15. Do QN, Lewis MA, Madhuranthakam AJ, et al. Texture analysis of magnetic resonance images of the human placenta throughout gestation: a feasibility study. *PLoS One*. 2019;14:e0211060. https://doi.org/10.1371/journal.pone.0211060
16. Andescavage N, Dahdouh S, Jacobs M, et al. In vivo textural and morphometric analysis of placental development in healthy & growth-restricted pregnancies using magnetic resonance imaging. *Pediatr Res*. 2019;85:974-981. https://doi.org/10.1038/s41390-019-0311-1
17. Shao Q, Xuan R, Wang Y, et al. Deep learning and radiomics analysis for prediction of placenta invasion based on T2WI. *Math Biosci Eng*. 2021;18:6198-6215. https://doi.org/10.3934/mbe.2021310
18. Hu Y, Chen W, Kong C, et al. Prediction of placenta accreta spectrum with nomogram combining radiomic and clinical factors: a novel developed and validated integrative model. *Int J Gynaecol Obstet*. 2023;162:639-650. https://doi.org/10.1002/ijgo.14710
19. Do QN, Lewis MA, Herrera CL, et al. Magnetic resonance imaging-based radiomics of axial and sagittal orientation in pregnant patients with suspected placenta accreta spectrum. *Acad Radiol*. 2025;32:1500-1505. https://doi.org/10.1016/j.acra.2024.09.045
20. Hutter J, Slator PJ, Jackson L, et al. Multi-modal functional MRI to explore placental function over gestation. *Magn Reson Med*. 2019;81:1191-1204. https://doi.org/10.1002/mrm.27447
21. Chen E, Mar WA, Horowitz JM, et al. Texture analysis of placental MRI: can it aid in the prenatal diagnosis of placenta accreta spectrum? *Abdom Radiol (NY)*. 2019;44:3175-3184. https://doi.org/10.1007/s00261-019-02104-1
22. Andescavage N, Kapse K, Lu YC, et al. Normative placental structure in pregnancy using quantitative magnetic resonance imaging. *Placenta*. 2021;112:172-179. https://doi.org/10.1016/j.placenta.2021.07.296
23. Sun H, Qu H, Chen L, et al. Identification of suspicious invasive placentation based on clinical MRI data using textural features and automated machine learning. *Eur Radiol*. 2019;29:6152-6162. https://doi.org/10.1007/s00330-019-06372-9
24. Zwanenburg A, Vallières M, Abdalah MA, et al. The image biomarker standardization initiative: standardized quantitative radiomics for high-throughput image-based phenotyping. *Radiology*. 2020;295:328-338. https://doi.org/10.1148/radiol.2020191145
25. van Griethuysen JJM, Fedorov A, Parmar C, et al. Computational radiomics system to decode the radiographic phenotype. *Cancer Res*. 2017;77:e104-e107. https://doi.org/10.1158/0008-5472.CAN-17-0339
26. Koçak B, Yüzkan S, Mutlu S, et al. Influence of image preprocessing on the segmentation-based reproducibility of radiomic features: in vivo experiments on discretization and resampling parameters. *Diagn Interv Radiol*. 2024;30:152-162. https://doi.org/10.4274/dir.2023.232543
27. Duron L, Balvay D, Vande Perre S, et al. Grey-level discretization impacts reproducible MRI radiomics texture features. *PLoS One*. 2019;14:e0213459. https://doi.org/10.1371/journal.pone.0213459
28. Dahdouh S, Andescavage N, Yewale S, et al. In vivo placental MRI shape and textural features predict fetal growth restriction and postnatal outcome. *J Magn Reson Imaging*. 2018;47:449-458. https://doi.org/10.1002/jmri.25806
29. Peng L, Yang Z, Liu J, et al. Prenatal diagnosis of placenta accreta spectrum disorders: deep learning radiomics of pelvic MRI. *J Magn Reson Imaging*. 2024;59:496-509. https://doi.org/10.1002/jmri.28787
30. Dong L, Lei Z, Zhang J, Sun Z, Li Y. Texture analysis of myometrium-derived T2WI in the evaluation of placenta increta: an observational retrospective study. *Placenta*. 2022;126:32-39. https://doi.org/10.1016/j.placenta.2022.06.002
31. Henson WH, Mazzá C, Dall'Ara E. Deformable image registration based on single or multi-atlas methods for automatic muscle segmentation and the generation of augmented imaging datasets. *PLoS One*. 2023;18:e0273446. https://doi.org/10.1371/journal.pone.0273446
32. Zou KH, Warfield SK, Bharatha A, et al. Statistical validation of image segmentation quality based on a spatial overlap index. *Acad Radiol*. 2004;11:178-189. https://doi.org/10.1016/s1076-6332(03)00671-8
33. Clark A, Flouri D, Mufti N, et al. Developments in functional imaging of the placenta. *Br J Radiol*. 2023;96:20211010. https://doi.org/10.1259/bjr.20211010
34. Bartels HC, O'Doherty J, Wolsztynski E, et al. Radiomics-based prediction of FIGO grade for placenta accreta spectrum. *Eur Radiol Exp*. 2023;7:54. https://doi.org/10.1186/s41747-023-00369-2
35. Wang Z, Jiao X, Liu W, et al. Comparative evaluation of clinical-MRI, radiomics, and integrated nomogram models for preoperative prediction of placenta accreta spectrum. *Acad Radiol*. 2025;32:2041-2052. https://doi.org/10.1016/j.acra.2024.10.021
36. Zou J, Wei W, Xiao Y, et al. Predicting placenta accreta spectrum and high postpartum hemorrhage risk using radiomics from T2-weighted MRI. *BMC Pregnancy Childbirth*. 2025;25:398. https://doi.org/10.1186/s12884-025-07516-0
37. Yu H, Yin H, Zhang H, et al. Placental T2WI MRI-based radiomics-clinical nomogram predicts suspicious placenta accreta spectrum in patients with placenta previa. *BMC Med Imaging*. 2024;24:146. https://doi.org/10.1186/s12880-024-01328-y

Downloaded from academic.oup.com/bjr/advance-article/doi/10.1093/bjr/tqag194/8767767 by guest on 30 September 2026

© The Author(s) 2026. Published by Oxford University Press on behalf of the British Institute of Radiology.
This is an Open Access article distributed under the terms of the Creative Commons Attribution License (https://creativecommons.org/licenses/by/4.0/), which permits unrestricted reuse, distribution, and reproduction in any medium, provided the original work is properly cited.
British Journal of Radiology, 2026, 00, 1–12
https://doi.org/10.1093/bjr/tqag194
Research Article

Downloaded from academic.oup.com/bjr/advance-article/doi/10.1093/bjr/tqag194/8767767 by guest on 30 September 2026